JVI Journals.ASM.org

# Cytoplasmic Trafficking, Endosomal Escape, and Perinuclear Accumulation of Adeno-Associated Virus Type 2 Particles Are Facilitated by Microtubule Network

**Ping-Jie Xiao[a,b] and R. Jude Samulski[a,c]**

Gene Therapy Center,[a] Department of Cell and Developmental Biology,[b] and Department of Pharmacology,[c] University of North Carolina at Chapel Hill, Chapel Hill, North Carolina, USA

**Understanding adeno-associated virus (AAV) trafficking is critical to advance our knowledge of AAV biology and exploit novel aspects of vector development. Similar to the case for most DNA viruses, after receptor binding and entry, AAV traverses the cytoplasm and deposits the viral genome in the cell nucleus. In this study, we examined the role of the microtubule (MT) network in productive AAV infection. Using pharmacological reagents (e.g., nocodazole), live-cell imaging, and flow cytometry analysis, we demonstrated that AAV type 2 (AAV2) transduction was reduced by at least 2-fold in the absence of the MT network. Cell surface attachment and viral internalization were not dependent on an intact MT network. In treated cells at 2 h postinfection, quantitative three-dimensional (3D) microscopy determined a reproducible difference in number of intracellular particles associated with the nuclear membrane or the nucleus compared to that for controls (6 to 7% versus 26 to 30%, respectively). Confocal microscopy analysis demonstrated a direct association of virions with MTs, further supporting a critical role in AAV infection. To investigate the underling mechanisms, we employed single-particle tracking (SPT) to monitor the viral movement in real time. Surprisingly, unlike other DNA viruses (e.g., adenovirus [Ad] and herpes simplex virus [HSV]) that display bidirectional motion on MTs, AAV2 displays only unidirectional movement on MTs toward the nuclei, with peak instantaneous velocities at 1.5 to 3.5 μm/s. This rapid and unidirectional motion on MTs lasts for about 5 to 10 s and results in AAV particles migrating more than 10 μm in the cytoplasm reaching the nucleus very efficiently. Furthermore, electron microscopy analysis determined that, unlike Ad and HSV, AAV2 particles were transported on MTs within membranous compartments, and surprisingly, the acidification of AAV2-containing endosomes was delayed by the disruption of MTs. These findings together suggest an as-yet-undescribed model in which after internalization, AAV2 exploits MTs for rapid cytoplasmic trafficking in endosomal compartments unidirectionally toward the perinuclear region, where most acidification events for viral escape take place.**

Adeno-associated virus (AAV), a member of the *Parvoviridae* family, is unique in that it requires helper virus (e.g., adenovirus [Ad] or herpes simplex virus [HSV]) for productive replication. This nonenveloped icosahedral protein capsid (~20 nm in diameter) packages a 4.7-kb single-stranded genomic DNA. The capsid is composed of three overlapping subunit proteins, encoded by the *cap* gene, at a Vp1/Vp2/Vp3 ratio of 1:1:10. Due to its unique properties, including nonpathogenicity, ability to transduce dividing and nondividing cells, breadth of tissue tropism, and sustainable transgene expression, several recombinant AAV capsids, especially serotype 2 (rAAV2), have been extensively exploited as gene therapy vectors (54). The potential of this vector has been well demonstrated by recent successes in several clinical trials, including treatment of Leber's congenital amaurosis (30) and hemophilia B (33). Despite many advances in vector development, administration of high-dose viral particles is required to achieve efficient transduction due to rate-limiting steps, including preexisting immune responses and nonspecific targeting (39). In addition to these limitations, the host cell also exploits various cellular components as barriers to productive AAV infection, including the critical steps required for viral trafficking (e.g., cell surface uptake, cytoplasmic trafficking, endosomal escape, nuclear entry, etc.) (53). Better understanding of the AAV cellular trafficking will advance our knowledge of AAV biology and facilitate the development of enhanced AAV vectors.

To successfully transduce a cell, AAV virions have to travel through a variety of cellular structures and organelles consecutively, including those involved in cell surface binding and internalization, cytoplasmic trafficking, and finally nuclear entry. It is known that AAV2 virions bind to their primary receptor, heparan sulfate proteoglycan (HSPG), on the cell surface (49) and are internalized through a clathrin-dynamin-mediated pathway (2, 12), which are facilitated by coreceptors, including integrins (48) and fibroblast growth factor (FGF) receptors (36). After entry, the virus remains associated with endosomes until acidification of the compartment, which triggers exposure of the N terminus of Vp1 protein (46). The N terminus of Vp1 carries phospholipase activity and facilitates escape of viral particles by breaking down the endosomal membrane (46). Successful transduction of AAV requires that its genome be delivered into the nucleus, which is believed to be achieved by nuclear localization signals on the capsid subunit Vp1 (19). However, little is known about how the viral particles traverse across the dense cytoplasm microenvironment from the cell periphery to the proximity of the nucleus, where AAV enters the nucleus.

**Received** 15 April 2012 **Accepted** 6 July 2012
**Published ahead of print** 18 July 2012
Address correspondence to R. Jude Samulski, rjs@med.unc.edu.
Supplemental material for this article may be found at http://jvi.asm.org/.

doi:10.1128/JVI.00935-12

Microtubules (MTs) are a component of cytoskeleton and are rope-like polymers of tubulins. MTs are highly dynamic, as characterized by alternate phases of elongation and shrinkage, and play critical roles in a variety of cellular processes, including maintaining cell structure, intracellular transportation, and forming the spindle during mitosis, to name a few (8). Their actions in intracellular transport are usually achieved by either their own growth dynamics (40) or the activities of associated motor proteins, particularly kinesin and dynein (29). Numerous studies have shown that both nonenveloped and enveloped viruses utilize MTs in infecting their host cells. This is typically exemplified by the utilization of dynein by viral particles to traffic through the crowded cytoplasmic environment to the nucleus. For AAV, previous studies have reported that MT disruption impairs AAV transduction (41) and that AAV can bind the cytoplasmic dynein in an *in vitro* binding assay (25). However, these studies were in contrast to another publication, which reported that AAV transduction was not affected by the disrupted MT network or dynein motor activity (21). As a result, the exact roles of MTs in AAV transduction as well as the underling mechanisms are yet unclear.

In this study, we have investigated the exact role(s) of MTs in AAV transduction and corresponding potential mechanisms using multiple techniques, including confocal microscopy, live-cell imaging, quantitative three-dimensional (3D) microscopy, pharmacological reagents, and single-particle tracking (SPT). Data from live-cell imaging and flow cytometry analysis demonstrated that the viral transduction was impaired in the presence of several chemicals used to disrupt MTs. This result was further supported by the measurements from quantitative microscopy, indicating that the proportions of AAV particles associated with the nuclear envelope or inside the nucleus were significantly diminished upon MT disruption. In single-particle tracking experiments, we observed that AAV virions display three classical types of particle motions, i.e., confined diffusion, normal diffusion, and directed motion. For the first time, we demonstrated the fast and unidirectional migration of AAV2 on MTs, with a peak instantaneous velocity of up to 1.5 to 3.5 μm/s, which is consistent with the motion mediated by the dynein motor. Furthermore, our observations from electron microscopy and pharmacological studies determined for the first time that AAV2 traffics on MTs in the endosomal compartment and that acidification of such structures is dependent on intact MTs. Together these data strongly support an as-yet-undocumented model in which AAV2 exploits MTs for its rapid directed cytoplasmic transportation toward the perinuclear sites where acidification of endosomes for viral escape takes place.

## MATERIALS AND METHODS

**AAV2 production, purification, and labeling.** AAV2 was produced in HEK-293 cells as previously described (18). Briefly, cells were transfected with three plasmids, pXR2, pXX680, and pTR-CMV-GFP (containing the green fluorescent protein [GFP] reporter transgene flanked by two inverted terminal repeats (ITRs). At 60 h after transfection, cells were harvested and nuclei were isolated using hypotonic buffer and a Kontes homogenizer (18). AAV2 particles were recovered by resuspending the nuclear pellet in phosphate-buffered saline (PBS) with 0.5% deoxycholate (DOC) and then sonicated for 1 min. Highly pure virus was then retrieved as described previously (55). Briefly, after DNase treatment, the virus suspension was subjected to one round of cesium chloride (CsCl) step gradient density fractionation and another round of fractionation using CsCl continuous gradient density. Determination of peak viral fractions, dialysis of virus, and measurement of viral titers by quantitative PCR (qPCR) were done as described previously (18). The infectivity of AAV has been determined to be about 1 transduction unit per 100 particles.

AAV2 was covalently labeled with Cy5 or 1.4-nm nanogold particles as described in the manufacturer's protocol with slight modifications. Briefly, purified AAV2 was incubated for 2 h at 4°C in PBS with a 20-fold molar excess of mono-NHS-Cy5 (GE Healthcare) or mono-NHS-nanogold (Nanoprobes) over the capsid protein units. Free dyes or nanogold was removed from labeled viral particles by dialysis against PBS containing 5% sorbitol, and viral solutions were stored at −80°C as small aliquots. The degree of labeling (DOL) of Cy5-AAV2 was determined by spectrophotometry according to the manufacturer's instructions. Titers of labeled virus were determined by both dot blotting (18) and qPCR. Infectivity of the viral particles was determined by GFP reporter gene assay.

**Cell culture and drug treatment.** HeLa cells (American Type Culture Collection) were grown in Dulbecco's modified Eagle medium (DMEM) (Invitrogen) with 10% fetal bovine serum (FBS) in a 5% $CO_2$ incubator. All cells were passaged every 2 to 3 days for up to 10 passages, and new aliquots of frozen cells were recovered from liquid nitrogen. To disrupt microtubules, the cells were incubated with medium containing 30 μM nocodazole or 10 μM vinblastine for 30 to 60 min before experiments. For lysosomotropic reagents, 50 μM chloroquine or 64 nM bafilomycin A1 was administered to block the acidification of endosomes. The drugs were maintained in the culture throughout the experiments.

**Pulse infection and immunofluorescence.** Pulse infection with AAV2 was performed as previously described (55). Briefly, HeLa cells were seeded on 12-mm glass coverslips at 24 h before infection. The next day, after incubation in DMEM containing 20 mM HEPES at 4°C for 5 min, cells were inoculated with Cy5-AAV2 (~5,000 viral genomes [vgs]/cell) at 4°C for another 40 min. Cells were washed with PBS to remove unbound virions and transferred to a 37°C incubator (this was regarded as 0 h postinfection [p.i.]).

For immunofluorescence, cells were washed with PBS and then fixed with 4% paraformaldehyde (PFA) for 15 min at room temperature (RT). The cells were then permeabilized with 0.2% Triton X-100 in PBS for 5 min at RT. After blocking with immunofluorescence buffer (IFB) (5% normal goat serum in PBS containing 0.05% Tween 20) for 1 h at RT, the cells were incubated with primary antibody to detect tubulin (rat monoclonal antibody from Abcam Inc.), diluted in 50% IFB, overnight at 4°C. The cells were then incubated in secondary antibody, diluted 1:2,000 in 50% IFB (anti-mouse Alexa-Fluor 488 [Molecular Probes]), for 1 h at RT. After six washes with PBS, coverslips were mounted cell side down on glass slides with mounting medium (Prolong Antifade Gold with DAPI [4′,6′-diamidino-2-phenylindole]; Molecular Probes).

**Reporter gene assay and live-cell imaging.** At 3 h after pulse infection with self-complementary AAV2 containing TR-CMV-GPF, HeLa cells were transferred to the stage of an Olympus IX-70 instrument for recording the GFP expression in real time. The camera was set to take a frame of GFP expression in dimethyl sulfoxide (DMSO)- or nocodazole-treated cells every 5 min. The snapshots of GFP expression were taken at the indicated time points from the video, and the level of GFP expression was measured by the mean fluorescence intensity (MFI) of GFP using the Image J program.

**Quantitative 3D microscopy.** HeLa cells pulse infected with Cy5-AAV2 were fixed with PFA and mounted on glass slides as described above. The distribution of viral particles in HeLa cells was examined using a Zeiss LSM710 laser scanning confocal microscope equipped with a Plan-Apochromat 63× 1.40-numerical aperture (NA) oil objective. Stacks of 20 to 30 focal planes were captured at 0.31-μm *z* intervals through the depth of the cell. 3D images of the cells were reconstructed by using the image stacks. All images were acquired at pixel dimensions of 0.13 by 0.13 by 0.31 μm (*x*, *y*, and *z*, respectively) to fulfill the Nyquist sampling.

Deconvolution was performed with AutoDeblur software (Media Cybernetics Inc.) using iterative and constrained algorithms as described

previously (55). The procedure started with a theoretical point spread function (PSF) derived from the actual setting of the Zeiss 710 confocal microscope, including the NA of the microscope objective, refractive index of the medium, excitation wavelength, emission wavelength, confocal pinhole radius, pixel size, *z*-axis interval, and microscope type (i.e., wide field, confocal). A new adjusted adaptive PSF derived from the previous deconvolution round was used to generate the next adaptive PSF that fit the real imaging data better than the previous one (termed one iteration or deconvolution round). A 12-round iteration was used to deconvolve all the confocal images in this study.

All deconvolved image stacks was processed using the IMARIS software package (Bitplane AG, Zurich, Switzerland) for visualization and quantification as described previously (55). Briefly, each deconvolved image stack was reconstructed using a volume-rendering module and smoothed by a 3D median filter. Subsequently, an isosurface-rendering module was applied through thresholding by the fluorescence intensity that is slightly higher than background. For Cy5-AAV2, the isosurface rendering was thresholded at the fluorescence intensity of 1,500 arbitrary units (a.u.) (the upper boundary of background). For DAPI, isosurface rendering was thresholded at the fluorescence intensity of 2,900 a.u. Parameters (volume, MFI, and total fluorescence intensity [TFI]) for these isosurface-coated Cy5-AAV2 objects were extracted from the IMARIS program and analyzed to determine the localization of particles as described previously (55).

**Internalization assay.** Pulse infection and immunofluorescence were carried out on HeLa cells as described above, except that the cells were not permeabilized when incubating with mouse monoclonal antibody A20 to specifically probe the viral capsids on cell surface. The colocalization between A20 and Cy5 signal was examined by 3D microscopy as described above. In this scenario, A20-positive Cy5-AAV2 presents the virion on cell surface, and A20-negative Cy5-AAV2 presents the virion inside the cells.

**Single-particle tracking and analysis.** For fluorescence imaging, HeLa cells were cultured in phenol red-free DMEM with 10% FBS in petri dishes with poly-L-lysine-coated glass coverslips on the bottom. Before fluorescence experiments, cells were washed in serum-free, phenol red-free medium supplemented with 20 mM HEPES (pH 8.0). The movement of Cy5-AAV2 particles was recorded with an Olympus IX-81 microscope equipped with a Hammatsu camera.

The trajectories of AAV particles were generated by the "cell" module in the IMARIS program. The location of each viral particle was computed as the centroid of the bright spot. The parameters (instantaneous speed, displacement, and displacement length) of the viral trajectories were directly extracted from the program as follows: instantaneous speed at time index $t$, $S(t) = \frac{\sqrt{D_x(t,t-1)^2 + D_y(t,t-1)^2}}{T(t) - T(t-1)}$, with $D_x(t_1,t_2) = P_x(t_1) - P_x(t_2)$ where $T(t)$ is time in seconds at time point $t$ and $P_x(t)$ is the $x$ position of the particle at time index $t$; displacement of particle at time $\Delta t$ after initial time point $t_0$, $D^2(\Delta t) = D_x{}^2(t_0 + \Delta t,t_0) + D_y{}^2(t_0 + \Delta t,t_0)$; and displacement length of a viral trajectory, $D(t_L,t_0) = \sqrt{D_x(t_L,t_0)^2 + D_y(t_L,t_0)^2}$, where $t_L$ is the last time index of the trajectory.

Mean square displacement (MSD) plot analysis was carried out as described previously (1, 7). For each trajectory of an AAV particle, the MSD for each time interval was calculated by the following formula: $\mathrm{MSD}(n\cdot\Delta t) = \frac{1}{N-n}\sum_{i=0}^{N-n-1}\{[D_x(i\cdot\Delta t + n\cdot\Delta t,i\cdot\Delta t)]^2 + [D_y(i\cdot\Delta t + n\cdot\Delta t,i\cdot\Delta t)]^2\}$, where $N$ is the total number of frames in the video, $\Delta t$ is the time interval between two successive frames, and $n$ and $i$ are positive integers.

**TEM.** For negative staining of AAV2 and nanogold-AAV2, viral particles in PBS were pipetted onto a glow-discharged copper grid. The grid was washed twice with water and then stained with 2% uranyl acetate. For visualizing nanogold-AAV2 in cells, infected HeLa cells were fixed at room temperature in 2% glutaraldehyde (in 0.15 M sodium phosphate buffer, pH 7.4) for 20 to 30 min, followed by 1 h in 1% OsO4. Silver enhancement was applied on the ultrathin sections. Electron microscopy images were taken with an LEO EM910 transmission electron microscope (TEM) at various magnifications.

## RESULTS

**Microtubule disruption impairs AAV2 transduction.** The microtubule (MT) network has been shown to be required for successful infection and replication of viruses, including canine parvovirus (CPV) and bovine parvovirus (BPV). To investigate the role of MTs in AAV infection, we first examined whether MT disruption affects viral transduction. Recombinant AAV2 (rAAV2) carrying a self-complementary GFP transgene cassette was used in reporter gene assays to evaluate the level of viral transduction. Self-complementary AAV2 (scAAV2) was designed to overcome the step of second-strand synthesis of viral DNA for successful transduction (31). AAV2 particles were incubated with cells at 4°C for about 40 min, and unbound particles were then removed by washing before cells were transferred to 37°C for subsequent viral events. This procedure is defined as "pulse infection" to synchronize viral infection, which was used in all experiments throughout this study. In this study, we used mean fluorescence intensity (MFI), reflecting the average number of GFP molecules per cell, to measure the level of AAV2 transduction. To better understand the viral transduction profiles, videos were taken on an IX70 microscope to record the expression of the viral GFP transgene in real time. Briefly, at 3 h after pulse infection with scAAV2-GFP, HeLa cells were transferred to the microscope stage for live imaging up to 21 h p.i. (see Movies S1 and S2 in the supplemental material). Snapshots were taken from the videos at 3 h, 6 h, 8 h, 12 h, 16 h, and 21 h after infection (Fig. 1A). The GFP expression by AAV2 could be detected as early as 6 to 8 h p.i. in DMSO-treated cells but was only barely detectable at 8 h p.i. in nocodazole-treated cells. The quantitative data on the GFP mean fluorescence intensity (MFI) agree with this observation (Fig. 1B). To test whether nocodazole reduces AAV transduction in a viral dose-dependent manner, different multiplicities of infection (MOIs) of AAV were used to pulse infect the HeLa cells in the presence of nocodazole or DMSO and GFP expression was measured by flow cytometry. To exclude the potential effects of dead cells on the quantification, we washed the cells in each well three times with PBS before harvesting them for flow cytometry analysis to remove any floating or loosely attached cells (which typically are dead ones). With this experimental procedure, we ensured that about 95% of the cells subjected to flow cytometry analysis were viable (data not shown). The histogram in Fig. 1C demonstrates that nocodazole treatment before AAV inoculation reduced the viral transduction at all tested dosages from 80 vgs/cell to 10,000 vgs/cell (Fig. 1C; see Fig. S1 in the supplemental material). There was no significant difference between pulse infections at 37°C and at 4°C in regard to the reduction of viral transduction by nocodazole treatment (Fig. 1C; see Fig. S2 in the supplemental material).

Nocodazole-induced MT disassembly could have reduced the viral transduction by impairing either the viral trafficking or the promoter activity of the transgene cassette. To examine the potential effects of nocodazole on the promoter activity of the AAV transgene cassette, we measured the GFP expression from plasmid transfection of a corresponding transgene cassette in AAV in the presence of DMSO or nocodazole. Our data show that level of GFP expression from plasmid transfection in the nocodazole-treated cells is not significantly different from that in DMSO-treated cells

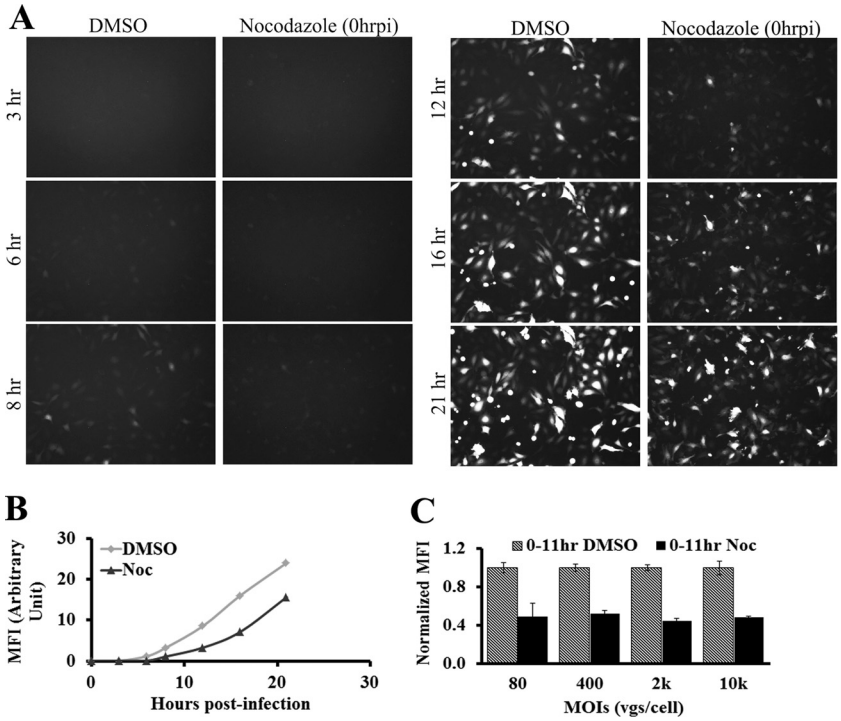


**FIG 1** Microtubule disruption before viral inoculation reduces early AAV2 transduction. At 30 to 60 min after pretreatment with DMSO or nocodazole, HeLa cells were incubated with AAV2-CMV-GFPsc (scAAV2-GFP) particles at 4°C for 40 min, and unbound virions were washed out before transferring HeLa cells to 37°C ("pulse infection"). A video of the GFP expression was taken from 3 h to 21 h after pulse infection. (A) Snapshots of the video were taken at 3, 6, 8, 12, 16, and 21 h p.i. (B) Quantification of GFP fluorescence intensity in the snapshots with Image J. (C) HeLa cells were treated with DMSO or nocodazole at 30 to 60 min before pulse infection with scAAV2-GFP at different dosages (80, 400, 2,000, and 10,000 vgs/cell). GFP expression was measured by flow cytometry at 11 h p.i., and mean fluorescence intensity (MFI) was normalized to that of DMSO treatment. The normalized ratio of the percentage of GFP-positive cells is shown in Fig. S1 in the supplemental material.

(see Fig. S3 in the supplemental material). This observation suggests that nocodazole treatment does not alter the activity of the promoter in the transgene cassette but instead affects the AAV transduction, most probably at the level of viral trafficking or processing. Importantly, the reduction of viral transduction was not limited to the nocodazole treatment but was also observed with other MT disassembly drugs, including colchicine and vinblastine (see Fig. S4 in the supplemental material). This result further demonstrates that it is MT disruption and not a side effect of nocodazole that impairs the viral transduction.

**AAV2 attachment and internalization on the cell surface are not affected by MT disruption.** MTs have been previously demonstrated to be critical for clathrin-dynamin-mediated viral entry as well as cytoplasmic trafficking of viruses (6, 15, 16, 51). Here we examined whether intact MTs are required for the attachment and internalization of AAV2 particles on the cell surface. Immediately after pulse infection, cells were harvested and subjected to viral genome extraction. The average number of viral genomes per cell was measured by quantitative PCR (Fig. 2A). The histogram in Fig. 2A shows that the amount of viral particles attached to the nocodazole-treated cells is comparable to that attached to control cells, demonstrating that an intact MT network is not required for cell surface binding of AAV2. To test whether internalization of AAV2 particles was affected by the disruption of MTs, we employed both Cy5-AAV2 particles and a mouse monoclonal antibody, A20, which can specifically recognize intact viral particles. For immunofluorescence on the cells with an intact cell membrane before permeabilization, antibody will not be able to enter the cell and will probe only the viral particles on cell surface. Under this scenario, HeLa cells were pulse infected with Cy5-AAV2 and fixed with paraformaldehyde at 0 h or 1 h after infection. Without permeabilization, cells were probed with A20 antibody and colocalization between Cy5 and A20 signal was imaged with confocal microscopy (Fig. 2B). The Cy5 signal represents all the viral particles on the cell surface and inside the cells, and the A20 signal highlights only the viral particles on the cell surface. As a result, A20-positive Cy5-AAV2 particles are on the cell surface and A20-negative Cy5-AAV2 particles are internalized inside the cells (Fig. 2C). Maximum-intensity projection (MIP) was applied to display 3D information of colocalization between A20 and Cy5 signals in 2D images (Fig. 2B). Figure 2B shows that almost all Cy5-AAV2 particles were also stained with A20 antibody on both control and nocodazole-treated cells at 0 h after infection, which is consistent with the fact that almost all viral particles should be on the cell surface without internalization at 0 h p.i. At 1 h p.i., the majority of Cy5-AAV2 particles were not stained with A20 antibody and only about 12% of viral particles were stained with A20 in the nocodazole-treated cells, a level which is comparable to that in control cells (Fig. 2B and C). These data determine that neither binding nor internalization of AAV2 particles on the cell surface is dependent on an intact MT network.

**MT disruption reduces the perinuclear accumulation and nuclear entry of AAV2.** The above-described results demonstrate that MT disruption before viral inoculation reduced the viral

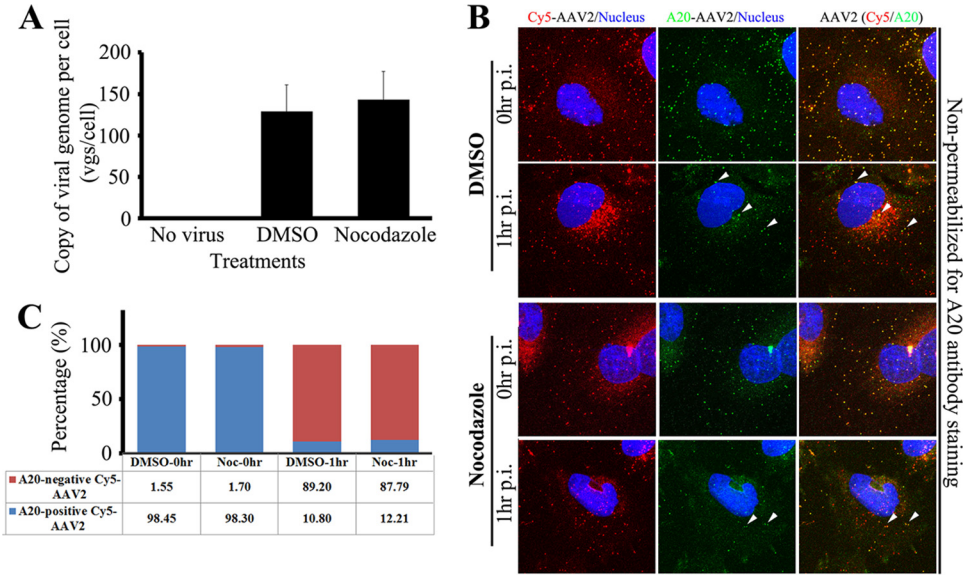


**FIG 2** MT disruption does not impair the attachment and internalization of AAV2. HeLa cells were preincubated with DMSO or nocodazole for 30 to 60 min before pulse infection with Cy5-AAV2. (A) To determine the binding efficiency, cells were harvested at 0 h p.i. for viral genome extraction. The number of viral genomes per cell (vgs/cell) was determined by quantitative PCR. (B and C) Cells were fixed at 0 h or 1 h p.i. without permeabilization. Nuclei were stained with DAPI (blue), and AAV2 capsids were stained with monoclonal antibody A20 (green). Before membrane permeabilization, A20 antibody is not able to access the viral particles inside the cells and thus binds only to the uninternalized AAV2 virions (yellow in the merged figures). (B) Representative images from maximum-intensity projection (MIP) show the costaining between A20 and Cy5 signals. Several representative uninternalized AAV2 particles are highlighted by arrowheads. (C) Quantification of colocalization between Cy5 and A20 as a measurement of viral particles remaining on cell surface and those which have internalized.

transduction by at least 2-fold and that neither viral attachment nor internalization was impaired by nocodazole treatment, suggesting that the reduced transduction is more likely caused by altered viral trafficking or processing (i.e., cytoplasmic trafficking or nuclear entry). For most DNA viruses, cytoplasmic trafficking from the cell periphery to the perinuclear region is critical for the nuclear entry of viral components. As nuclear entry of AAV2 is known to be a prerequisite for successful viral transduction, we examined the efficiency of these events under nocodazole or DMSO treatment. Here, we used Cy5-AAV2 particles generated by covalent labeling of purified AAV2 capsids with Cy5 fluorophores as described previously (55). After pretreatment with nocodazole or DMSO for 30 to 60 min to allow full disruption of MTs by nocodazole, HeLa cells were pulse infected with Cy5-AAV2 and the localization of viral particles was examined at 2 h p.i. using confocal fluorescence microscopy (Fig. 3; see Movies S3 and S4 in the supplemental material). Figure 3A shows a representative distribution of AAV2 particles upon DMSO or nocodazole treatment for 2 h. To quantify such a distribution, we used 3D quantitative microscopy as described previously (55), and Fig. 3B shows representative images to illustrate the actual quantification by presenting the views from different angles of the 3D images (Fig. 3B; see Movies S3 and S4 in the supplemental material). The quantitative data are presented in Fig. 3C. In DMSO-treated cells, AAV2 particles were distributed normally; i.e., about half of the intracellular particles localized at the nuclear periphery, 10 to 15% were in the nucleus (with 39 particles per nucleus on average), and the remaining particles were in the cytoplasm (Fig. 3B and C). In the cells where MTs were fully disrupted by nocodazole, only about 3% of viral particles were in the nucleus (about 12 particles per nucleus on average), and the remaining 97% of the particles were scattered across the cytoplasm (Fig. 3B and C). In the aspect of nuclear targeting, viral particles seem to get lost in the cytoplasm and randomly localize in the nocodazole-treated cells. It is known that the nuclear envelope is one of the cellular structures that AAV2 particles have to interact with before their nuclear entry. Figure 3 clearly shows that a much smaller proportion of intracellular AAV2 virions localized at the perinuclear region in the nocodazole-treated cells than in the DMSO-treated cells (Fig. 3A and B). We then tested whether reduced perinuclear localization of AAV2 had led to a reduced proportion of virions associated with the nuclear membrane. Using the quantification method established previously (55), we determined that only about 3% of AAV2 particles associated with the nuclear membrane in the nocodazole-treated cells, compared to over 10% in the control cells (Fig. 3C). These data suggest that the cytoplasmic trafficking from the cell periphery to the perinuclear region may facilitate interaction of the virus with the nuclear membrane. All of these data support a model where MT disruption reduces the proportions of AAV2 particles in the perinuclear and nuclear regions and thus reduces the viral transduction.

**AAV2 exploits MTs for rapid and unidirectional trafficking from cell periphery to perinuclear region.** The reduced perinuclear accumulation and nuclear entry are most likely caused by the impaired MT-mediated cytoplasmic trafficking, as evidenced for other viruses (16, 28, 45). To further investigate the potential role of MTs in AAV2 infection, we first examined the colocalization between virions and MTs in cells. At 30 min or 2 h after pulse infection with Cy5-AAV2, HeLa cells were fixed with paraformaldehyde and MTs were probed with α-tubulin antibody. A confocal microscope was used to image the localization of AAV2 particles on MT filaments (Fig. 4). At 30 min p.i., the majority of AAV2 was localized on the MTs at the cell periphery. At 2 h p.i., about 30% of viral particles were localized on the MTs at the cell periph-

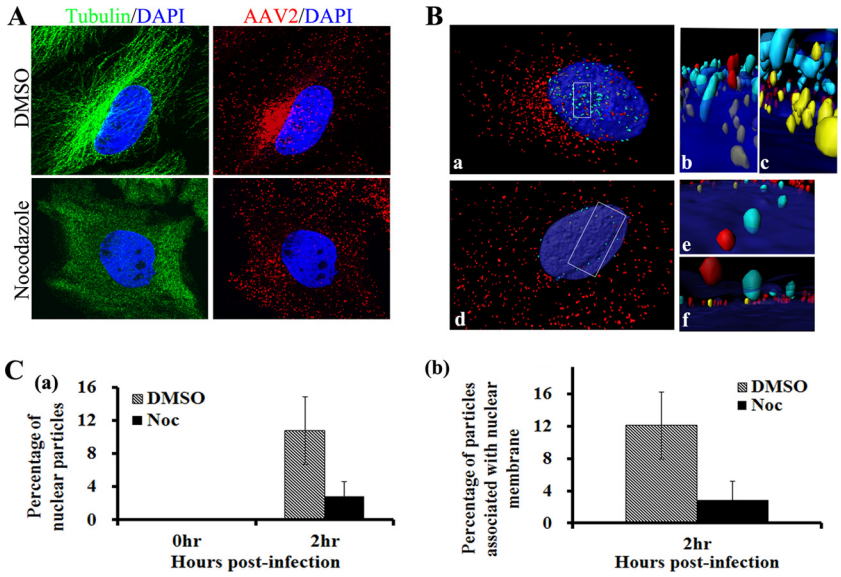


**FIG 3** Early perinuclear accumulation and nuclear entry are reduced by the disruption of the MT network. HeLa cells were preincubated with DMSO or nocodazole at 30 to 60 min before the pulse infection with Cy5-AAV2. Cells were fixed at 0 h or 2 h p.i. Nuclei were stained with DAPI (blue), and MTs were stained with alpha-tubulin antibody (green). (A) Representative 2D images show the distribution of Cy5-AAV2 particles (red) at 2 h p.i. in the cells treated with DMSO or nocodazole. (B) Representative images illustrate the quantification of viral distribution using 3D microscopy in the cells treated with DMSO (panels a to c) or nocodazole (panels d to f) as described previously (55). Panels a and d, top views; panels b to f, magnified side views of the insets in panels a and d; panels b and e, side views observed above the nucleus (the nuclear envelope is indicated by the blue layer, based on the DAPI signal); panels c and f, side views observed inside the nucleus (between the top and bottom nuclear envelopes). AAV2 particles in cytoplasm are highlighted as red, these associated with the nuclear envelope are cyan, and these inside the nucleus are yellow. More details about the viral distribution in these cells are shown in Movies S3 and S4 in the supplemental material. (C) Percentages of AAV2 particles in the nuclei (panel a) and associated with the nuclear envelope (panel b), calculated from 15 to 20 cells in each group based on the quantification illustrated in panel B).

ery, about 50% of viral particles had finished trafficking from the cell periphery to the perinuclear region, and over 10% of intracellular particles had entered the nucleus (Fig. 4) (55).

Next, we tested whether the role of MTs during AAV infection is at the step of cytoplasmic trafficking from the cell periphery to the perinuclear region. To this end, single-particle tracking (SPT) in live cells was used to study the trafficking of AAV2 in the cytoplasm. From previous SPT studies of other viruses, including Ad and influenza virus (1, 26), it is known that cytoplasmic transportation is usually characterized by fast and directional movements on MT filaments. In our SPT experiments with the nontreated cells, Cy5-AAV2 particles displayed rapid and unidirectional movements from the cell periphery to the perinuclear region (Fig. 5A and B; see Movie S5 in the supplemental material). This is different from the bidirectional movement of Ad or HSV on MTs. Figure 5A suggests that such directed motion is on the MT tracks. Consistent with previous studies of MT-mediated trafficking (26), the Cy5-AAV2 particles migrated with instantaneous velocities of 1.5 to 3.5 μm/s when moving from the cell periphery to the perinuclear region (Fig. 5C). This movement persisted for only 5 to 10 s (Fig. 5C) and allowed for a large displacement between the initial and final positions of the particle (Fig. 5D, panel a). Mean square displacement (MSD) analysis was employed to verify that the observed motion of the Cy5-AAV2 particles is an active transportation event rather than passive diffusion of virions in the cytoplasm. MSD analysis is typically used to describe three types of particle motions: confined diffusion, normal diffusion, and directed motion (Fig. 6B). Active transportation on MTs is one type of directed motion, which can be described by a quadratic dependence of MSD on time interval $\Delta T$ (Fig. 6B). The MSD-$\Delta T$ plot of the viral particle indicated by arrowheads in Fig. 5A can be fitted into a quadratic curve, demonstrating that the movement of this particle is directed motion and is consistent with dynein-mediated retrograde trafficking on MTs (Fig. 5D, panel b).

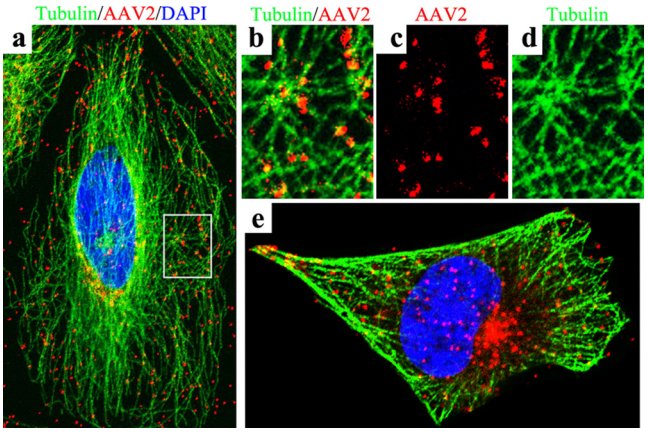


**FIG 4** AAV2 colocalizes with MTs. Cells were fixed at 30 min (a to d) or 2 h (e) after pulse infection with Cy5-AAV2. The nucleus was stained with DAPI (blue), and MTs were stained with alpha-tubulin antibody (green). The localization of Cy5-AAV2 (red) on MTs (green) is shown in panels a and e. Panels b to d show magnified views of the inset in panel a.

**Rapid directional motion of AAV2 particles is ablated by MT disruption.** To further verify that such directed movement is mediated by MTs, we examined the viral trafficking in the presence of nocodazole. Videos of viral trafficking were taken at 1 to 1.5 h after

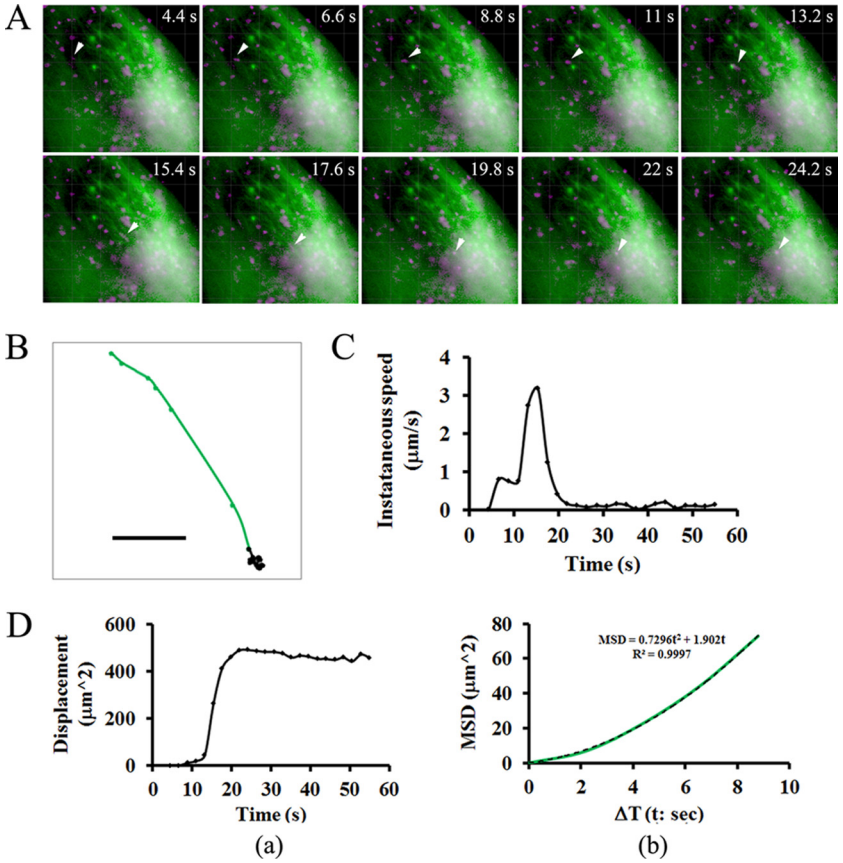


**FIG 5** Fast and unidirectional movement of AAV2 toward the perinuclear region. Videos were taken at 1 h after pulse infection with Cy5-AAV2 using an Olympus IX81 inverted fluorescence microscope. (A) Snapshots of consecutive frames with a 2.2-s time interval show the fast and directed movement of Cy5-AAV2 (purple and indicated by arrowheads) on microtubules (green) toward the perinuclear region. (B) Trajectory of the Cy5-AAV2 particle indicated by arrowheads in panel A. Frames subject to directional transport are shown as green points and lines, and those with confined motion in the perinuclear region are indicated as black points. The bar represents 5 μm. (C) Instantaneous velocity of the particle (indicated by arrowheads in panel A) over time. (D) The displacement from the starting position (panel a) and mean square displacement (MSD) (panel b) are plotted for the particle indicated by arrowheads in panel A. In panel b, the plot between MSD and time interval ($\Delta T$) is fitted by a quadratic curve (dashed line, MSD = $0.7269t^2 + 1.902t$) with $r^2 = 0.9997$.

pulse infection with Cy5-AAV2 particles at about 1 frame per second (see Movies S6 and S7 in the supplemental material). As shown in the movies in the supplemental material, compared with that in control cells, directional movement was completely ablated in the nocodazole-treated cells (Fig. 6A; see Fig. S5 in the supplemental material). Based on MSD plot analysis (Fig. 6B), the directed movement of AAV2 particles indicated by quadratic curve was observed only in the control cells and not in nocodazole-treated cells (Fig. 6C). Both normal diffusion characterized by linear dependence of MSD on $\Delta T$ and confined diffusion indicated by asymptotic behavior of MSD on $\Delta T$ were not disrupted in the presence of nocodazole. Particle motions with peak instantaneous velocities of over 1.5 μm/s were totally lost in the presence of nocodazole (Fig. 6D, panel a). Correspondingly, particles motions resulting in large displacement (>10 μm) responsible for particle transportation from the cell periphery to the perinuclear region were also observed only in the control cells and not in the cells lacking an intact MT network (Fig. 6D, panel b). The above data demonstrate that rapid and unidirectional trafficking of AAV2 from the cell periphery to the perinuclear region requires intact MTs. Our data also suggest that an intact MT network is unlikely to be involved in either confined or normal diffusion (Fig. 6C).

**AAV2 migrates on MTs in the endosomes, and the acidification of these structures is delayed by MT disruption.** After internalization through clathrin-dynamin-mediated endocytosis, several DNA viruses, including parvoviruses, have to escape from the endosomes upon the acidification of these membranous structures. It is known that adenovirus (Ad) escapes from the endosome in an early stage during infection (within 30 min p.i.) before these particles migrate on MTs (27, 28). In contrast, little is known about the timing of endosomal escape and MT-mediated trafficking of parvoviruses. Our electron microscopy data demonstrate that AAV2 particles were inside the endosomes when migrating on MTs (Fig. 7A). This observation is the first one to show that AAV2 particles, in contrast to Ads, usurp the MT-mediated endosomal trafficking for their nuclear targeting. It is also known that the maturation of endosomes takes place during their trafficking on MTs from the cell periphery to the perinuclear region, where most mature late endosomes with low pH locate (22, 52). We used pharmacological studies to further test whether MT-mediated transportation is required for the acidification of AAV-containing endosomes. Consistent with an earlier report (2), chemicals (bafilomycin and chloroquine) that block endosomal acidification inhibited AAV transduction (Fig. 7B, panel a). It was demonstrated previously that adenovirus escapes from early endosomes

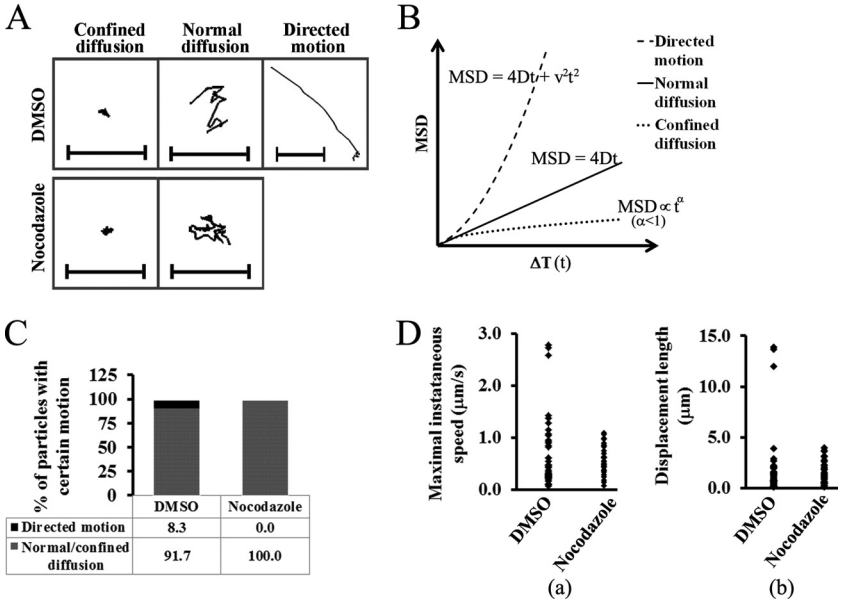


**FIG 6** Fast and unidirectional movement of AAV2 particles is dependent on intact microtubules. (A) Representative trajectories for AAV2 in DMSO- or nocodazole-treated cells as shown in Movies S6 and S7 in the supplemental material. Bars represent 5 μm. (B) Three simulated MSD plots for various types of particle motion. The mean square displacement (MSD) is plotted against time interval $\Delta T(t)$. Normal diffusion is usually described by a linear plot given by the formula MSD = $4Dt$ ($D$ is the diffusion coefficient). Directed motion is usually described by a quadratic curve given by the formula MSD = $4Dt + v^2t^2$ ($v$ is the mean velocity of the motion). An asymptotic behavior with MSD$\propto t^{\alpha}$ ($\alpha<1$) indicates confined diffusion. (C) Proportions of viral particles with directed motion or diffusion from MSD analysis. (D) Maximal instantaneous speed (panel a) and displacement length (panel b) of each AAV2 track. For panels C and D, trajectories were generated only for these viral particles continuously tracked over 20 frames, and about 40 to 60 trajectories were analyzed for each group.

before migrating on MTs, and its infection is not sensitive to the inhibition of endosomal acidification as early as 20 to 30 min after viral inoculation (4, 27). Notably, our data demonstrate that the infection of most AAV2 particles was still sensitive to bafilomycin and chloroquine at 1 h p.i. and that these reagents were still able to partially inhibit (20%) the viral transduction even when added at 2 h p.i. (Fig. 7B, panel a). This observation suggests that some postentry trafficking events, including MT-mediated migration,

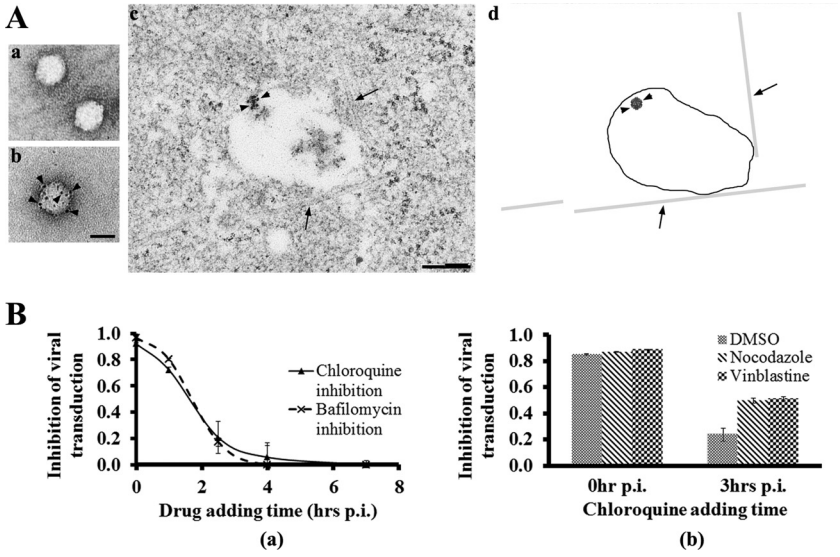


**FIG 7** Association of AAV2-containing endosomes with MTs and delayed endosomal acidification upon MT disruption. (A) AAV2 particles migrate on MTs in membranous structures. AAV2 particles before (panel a) and after (panel b) labeling of nanogold were demonstrated by TEM. Bar, 20 nm. A micrograph showing the direct association of AAV-containing endosome with MTs at 1 h after pulse infection of nanogold-labeled AAV2 (panel c) is simplified in a cartoon diagram (panel d). In the cartoon, MTs are indicated by arrows, the endosome membrane is indicated by closed line, and virus is indicated by arrowheads. Bar, 200 nm. (B) Acidification of virus-containing endosomes is inhibited by lysosomotropic chemicals at various time points after pulse infection of AAV2 (panel a). At 1 h after pretreatment with anti-MT drugs (nocodazole and vinblastine), chloroquine was added at 0 h or 3 h after pulse infection of AAV2. To calculate the inhibition of viral transduction, the expression level of GFP transgene was measured with a flow cytometer and normalized to corresponding treatments without chloroquine (panel b).

are required for at least a subset, if not all, of the viral particles before endosomal acidification to allow their escape from the late-stage endosomes. In concert with this scenario, disruption of MTs delays the acidification of AAV-containing endosomes and viral escape, as demonstrated by the data that administration of anti-MT reagents (nocodazole and vinblastine) resulted in an increased inhibition of viral transduction by addition of chloroquine at 3 h after pulse infection (Fig. 7B, panel b). This is consistent with earlier reports that AAV2 was routed to late endosomes for infection (9, 11, 55). These results suggest that AAV2 particles traffic on MTs in endosomes from the cell periphery to the perinuclear region, where acidification of these membranous structures and viral escape take place.

## DISCUSSION

Cytoplasmic trafficking is critical for most DNA viruses to approach the perinuclear region and deposit their genomic DNA in the nuclei of host cells. Previous studies have demonstrated that either actin filaments or microtubules (MTs) are exploited by various viruses to traverse the dense cytoplasm. For AAV, the exact mechanism of cytoplasmic trafficking of this virus remains unclear, as previous reports have been diametrically opposite in their conclusions (21, 25, 41). Here we have studied the role of MTs in AAV2 transduction and have extensively investigated the underlying mechanisms of how MTs contribute to viral infection, using various pharmacological and microscopy tools. Our data from live-cell imaging and flow cytometry analysis determined the involvement of MTs in AAV2 infection, and the data from quantitative 3D microscopy and quantitative PCR analysis demonstrated that an intact MT network is required for the nuclear targeting of AAV but not for cell surface attachment or endocytosis of this virus. In the present study, for the first time we have determined that the migration of AAV2 on MT tracks is fast (up to 1.5 to 3.5 μm/s), which is consistent with dynein-mediated trafficking, and is unidirectional, which is different from the bidirectional motion of Ad or HSV on MTs. In addition, our study using electron microscopy and pharmacological experiments is the first one to suggest that AAV traffics on MTs in endosomes and that acidification of these structures is dependent on an intact MT network. The findings herein strongly support an as-yet-undocumented model in which after internalization, AAV2 exploits MTs for fast and unidirectional trafficking in endosomal compartments toward the perinuclear region, where most viral acidification events take place. Furthermore, our data that MT disruption never completely blocks AAV2 transduction suggest the existence of an alternative, MT-independent trafficking pathway for this virus. These data together with earlier studies support a model of AAV2 trafficking during its early infection (Fig. 8) (9, 11, 23, 41).

Both DNA and RNA viruses hijack MTs to achieve productive infection in host cells. Several parvoviruses, including CPV and BPV, also have been shown to exploit the MT network for their transduction (13, 47). However, the role(s) of MTs in AAV infection remains controversial. To carefully examine the potential effect of MTs on AAV2 transduction, we employed live-cell imaging to monitor the dynamics of transgene GFP expression in real time as a measurement of successful viral transduction. In contrast to the case in the nontreated cells, where a GFP fluorescence signal was readily visible as early as 6 h p.i., GFP expression was much lower in the nocodazole-treated cells and was barely detectable until 8 h p.i. (Fig. 1A). This result is further confirmed by the flow

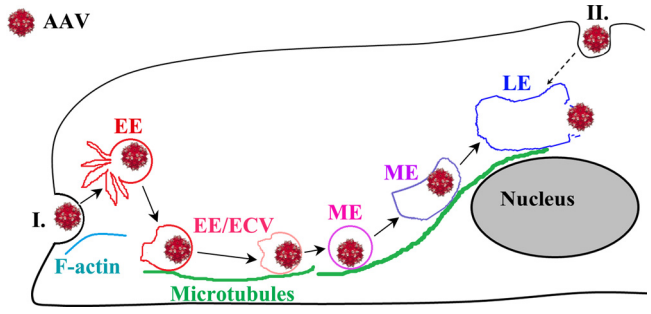


**FIG 8** A model for the role of microtubules in the cytoplasmic trafficking and endosomal acidification for AAV2 escape. After binding and endocytosis on the cell surface, AAV2 virions may take two possible trafficking routes toward the nucleus. Route I, for these internalized at sites distal from the nucleus, virions migrate on MT tracks in endosomes to traverse the dense cytoplasm toward the perinuclear regions of host cells. Route II, for these internalized at sites close to the nucleus, virions in endocytic vesicles can reach the nucleus by slower MT-independent migration through the cytoplasm between the cytoplasmic membrane and nuclear envelope. For both routes, acidification of the AAV2-containing endosomal compartment happens at the perinuclear region and allows the escape of viral particles from vesicles, a prerequisite step for nuclear entry.

cytometry data showing that the expression level of the GFP transgene is lower in MT-disrupted cells than in control cells (Fig. 1B). These observations are consistent with studies from Englehardt's group supporting the involvement of MTs in AAV transduction (41). In contrast, a previous report concluded that intact MTs were not involved in AAV infection as measured by the percentage of GFP-positive cells after inoculation of AAV-GFP (21). Interestingly, we also observed similar proportions of GFP-positive cells in both nocodazole- and DMSO-treated cells with high viral loading (5,000 to 10,000 vgs/cell), though the GFP signal was much weaker in nocodazole-treated cells than in control cells (Fig. 1A; see Fig. S1 in the supplemental material). It is known that only a few AAV2 particles in the nucleus are needed to turn a cell "green" (regardless of how faint this "green" is) and thereby for the cell to be identified by flow cytometry as a "GFP-positive cell" (references 5, 9, 24, and 31 and data not shown). In addition, our quantitative microscopy data demonstrated that MT disruption only reduced the nuclear entry of AAV2 and did not completely block this process (Fig. 3). Under this scenario, it is expected that only a decreased level of GFP fluorescence intensity and not a decreased percentage of GFP-positive cells will be observed if the reduced number of nuclear virions upon MT disruption is still high enough to turn a cell "green," which is particularly true when a high viral dosage is used (Fig. 1; see Fig. S1 in the supplemental material). As a result, GFP mean fluorescence intensity (MFI) is a more reliable measurement to assess AAV transduction in this study. Our data from multiple approaches, including live-cell imaging, flow cytometry analysis, and quantitative microscopy, have strongly suggested that AAV particles exploit the MT network during their infection. Additionally, MT disruption only reduced and did not fully block viral transduction and nuclear entry, which suggests the existence of an alternative but slower trafficking route(s) in addition to the MT network for AAV infection (Fig. 8). Exploration of this potential alternative pathway(s) should shed light on the dynamics of AAV infection in various cell types.

It was previously documented that after being disassembled by nocodazole or a cold temperature, the MT network can be made to

recover to the predrug level by either washing out the drug or rewarming the cells to 37°C within 10 to 20 min (4). We also observed the full recovery of the MT network from a cold temperature at about 30 min after incubation at 37°C (data not shown). Given that the flow cytometry assay was carried out at 10 to 12 h after pulse infection, the incubation of cells at 4°C for viral binding should have minimal effects on AAV2 transduction. Consistently, we did not observe a significant difference between pulse infections at 4°C and 37°C in regard to the reduction of viral transduction by nocodazole treatment (Fig. 1; see Fig. S2 in the supplemental material). To exclude the potential effect of dead cells on the viral transduction measurement, we washed the cells in each well three times with PBS before harvesting them for flow cytometry analysis to remove any floating or loosely attached cells. In this study, about 95% of cells used for flow cytometry analysis were viable as demonstrated by multiple methods, including trypan blue exclusion or 7-aminoactinomycin D (7-AAD) exclusion assays (data not shown). The results and conclusions presented in this study are not influenced by technical concerns such as a contribution of dead cell artifacts.

To specifically study the cytoplasmic trafficking of viral particles after internalization, we carried out single-particle tracking (SPT) experiments to trace virions at 1 to 1.5 h after infection (Fig. 5 and 6). Besides technical considerations associated with single-particle tracking experiments, 1 to 1.5 h p.i. is the better time to image MT-mediated AAV2 trafficking for two reasons: first, at this time point, almost all AAV2 particles are internalized (Fig. 2) and the observation of intracellular trafficking will not be confounded by the viral motions on the cell surface that typically happen at earlier time points, and second, the location of the microtubule-organizing center (MTOC) can be readily visualized by the perinuclear accumulation of AAV particles, which will allow one to determine if the MT-mediated migration is toward or away from the perinuclear region. As observed in other SPT studies (1), our SPT data show that about 8% of viral particles displayed rapid and directional motions with instantaneous speeds of up to 1.5 to 3.5 μm/s during our observation time in the normal cells. The remaining virions displayed either normal diffusion (Brownian motion) or confined diffusion, an indication of movement of AAV in cytoplasm or actin filaments. As it takes about 2 to 4 h for most virions to finish trafficking from the cell periphery to the perinuclear region (Fig. 4 and data not shown), it is expected that we will observe only a small subset of particles displaying rapid directional movements on MTs (each event persists for only 5 to 10 s) in the limited time window (on the order of a minute) that we can trace the virions in the single-particle tracking experiment. In addition, the live imaging allows one to image only a subset of viral particles on a certain focal plane in the cell, and inevitably the investigator will lose track of other viral particles moving in the same cell at a different plane. Furthermore, fast directional motion may be interrupted by temporary dissociation of the viral particle from MT tracks or alternatively stalled motors (dynein for minus-end-directed motion) (29, 50). Under these experimental limitations, the "8%" from single-particle tracking experiments does not precisely represent the portion of viral particles migrating on the MTs during the observation time, not along the entire viral trafficking period (several hours). Instead, this number is more to show the existence of MT-mediated fast and directional movements in the cells, compared with the complete absence of such motion in MT-disrupted cells. In all, the window of observation that we utilized, while short in duration, supported the rapid and unidirectional movement of AAV particles only when MTs were intact.

Interestingly, compared with those in control cells, AAV2 particles in a much smaller proportion were still detected in the nuclei of nocodazole-treated cells (Fig. 3). This is consistent with the observation in the reporter gene (GFP) assay that AAV2 was still able to transduce cells in the presence of nocodazole, though at a reduced level compared with that in control cells (Fig. 1). One possible reason for this observation is related to the inefficient MT-independent trafficking of virions. Under this scenario, AAV2 particles could be internalized in the cell membrane close to the nucleus, where the virions have to traverse only a small distance to reach the nucleus (Fig. 8) (29). Movements over such short distance (several micrometers) might be achieved by normal diffusion. Internalization in the sites around the nucleus can be achieved by the direct binding of viral particles at these sites (our unpublished data) or by viral surfing on the cell membrane to these sites (34). Our studies do not exclude the possibility that AAV2 particles may reach the nucleus through a much slower process by exploiting actin filaments or intermediate filaments (35, 43). Although it is not uncommon for viruses to exploit multiple pathways to ensure productive infection, we provide significant data to support the role of MTs, whereas other putative pathways require further investigation. All these possible scenarios allow motions with lower velocity and/or directionality toward the nucleus and are supported by our observation that early AAV transduction was delayed in the presence of nocodazole (Fig. 1A and B).

It was also reported that in an *in vitro* binding assay, cytoplasmic dynein can directly bind to AAV2 capsid (25). An interesting question is whether the rapid directed motion of AAV2 is mediated by the dynein associated with endosomes or by that directly associated with viral capsid. It is known that AAV2 is internalized through a clathrin-dynamin-mediated pathway into endosome compartments (2, 12). While we were not able to definitively determine dynein interaction with AAV-containing endosomes versus capsids specifically, our data strongly support the usage of this motor in fast directed movement of AAV. Interestingly, some dynactin subunits, such as p62, were demonstrated to have a minimal impact on dynein-mediated functions and were suggested to be dispensable for the function of the dynactin complex (37, 42). More importantly, recent studies have begun to demonstrate that dynein can directly bind to pathogen-related cargo, and they suggest that dynactin may be dispensable, especially for dynein-mediated pathogen trafficking (3, 20, 42). Careful and sophisticated investigations will be required to address the issues regarding whether and how the dynactin complex contributes to the MT-mediated AAV2 trafficking.

It was interesting to note that AAV particles employed endosomes for their transportation on MTs up to the perinuclear region. We have employed electron microscopy analysis to determine that AAV2 particles are in the endosomal structures when migrating on MTs (Fig. 7A). It is also known that acidification of endosomes is essential for escape of AAV2 from vesicles into the cytoplasm (2, 11). Our pharmacological study indicating that MT disruption prolonged the sensitivity of AAV2 infection to bafilomycin and chloroquine strongly suggests that prompt acidification of AAV-containing endosomal compartment requires intact MTs (Fig. 7B). These data altogether suggest an undescribed

model for AAV in which after internalization, AAV2 rapidly and unidirectionally traffics on MTs in endosomes directly toward perinuclear sites, where most viral acidification events happen. This model is in concert with the notion that most acidic endosomes are localized at perinuclear sites where viruses, such as influenza virus, escape from these membranous structures (26, 32). This model is also consistent with the earlier observations that AAV2 is associated with late endosomes (9) and that viral mutants (VP3-only and HD/AN) lacking phospholipase activity can be transported to the perinuclear region indistinguishably from parental virions (reference 23 and data not shown) but remain noninfectious. Interestingly, AAV's helper viruses, such as Ad and HSV, have been shown to exploit a different strategy. Instead of moving on MTs in membranous structures, both Ad and HSV have to escape from the endosomes before trafficking on MTs, which is consistent with their direct interaction with both minus-end-directed and plus-end-directed MT motor proteins, allowing the bidirectional motions documented for both Ad and HSV on these filaments (10, 14, 38). Typically, the infection by these viruses is not sensitive to the inhibition of endosomal acidification by bafilomycin or chloroquine as early as 20 to 30 min after viral inoculation (17). In contrast, AAV particles apparently traffic unidirectionally on MTs, as determined by the interaction between the virus-containing endosomes and dynein motors (26). Our data that the majority of AAV2 was still sensitive to both bafilomycin and chloroquine at 1 h p.i. imply that a more acidic environment is required for the exposure of Vp1 on viral capsids as well as the viral escape from these membranous structures (32), compared with the early escape of Ad and HSV from endosomes at the cell periphery (27, 44, 45). This result is consistent with the early notions that multiple viral components, including Vp1 and basic regions on capsid, have to externalize in the endosomes (46). The observation that 80% of AAV2 was insensitive to bafilomycin and chloroquine treatments at 2 h p.i. indicates that most virions have accomplished all these viral actions requiring endosomal acidification and even may have escaped from the late endosomes. These studies together suggest that the rapid directed motion of AAV2 happens when the viral particles are still inside the endosomes. It should be noted that our data do not exclude the possibility that some AAV2 can escape from the early endosome as an alternative pathway in the cells. Given that cytoplasmic dynein can directly bind to AAV2 capsids *in vitro* (25, 56), it will be of particular interest in the future to identify and mutate the dynein binding sites on AAV2 capsids and further investigate the trafficking of these mutant capsids. Furthermore, understanding the next steps of viral entry (i.e., nuclear entry transition from the perinuclear region) may give critical insights into mechanisms that can be exploited for more efficient vector transduction.

The findings reported here show that microtubule-dependent transport plays an essential role in viral transduction, especially the early onset of transgene expression. Importantly, the data in this study strongly support an as-yet-undocumented model in which after internalization, AAV2 exploits fast and unidirectional transportation on MTs in endosomes directly toward the perinuclear region, where acidification of most AAV-containing endosomal compartments happens. Validating trafficking pathways *in vivo* (55) should allow the research community to enhance the performance of viral vectors by manipulating intracellular events as documented in the *in vitro* studies.

## ACKNOWLEDGMENTS

This research was funded from NIH grants 1R01AI080726-01A2 and 1R01DK084033-01 (to R.J.S.).

We thank members of the UNC Gene Therapy Center, specifically Thomas Bridges Lentz and Angela Mitchell, for productive discussions. We also thank members of the laboratory of Ken Jacoboson, especially Ken Jacobson and Michelle Itano, for providing informative suggestions. We thank Lu Huang in the Cystic Fibrosis Center for statistical data analysis. We greatly appreciate Swati Yadav for calculating virus titers by qPCR. We also thank the members of the Microscopy Services Laboratory, especially Robert Bagnell, Steven Ray, and Victoria Madden, for providing resources.

## REFERENCES

1. **Akita H, et al.** 2010. Particle tracking of intracellular trafficking of octa-arginine-modified liposomes: a comparative study with adenovirus. Mol. Ther. **18**:955–964.
2. **Bartlett JS, Wilcher R, Samulski RJ.** 2000. Infectious entry pathway of adeno-associated virus and adeno-associated virus vectors. J. Virol. **74**: 2777–2785.
3. **Bremner KH, et al.** 2009. Adenovirus transport via direct interaction of cytoplasmic dynein with the viral capsid hexon subunit. Cell Host Microbe **6**:523–535.
4. **Cassimeris LU, Wadsworth P, Salmon ED.** 1986. Dynamics of microtubule depolymerization in monocytes. J. Cell Biol. **102**:2023–2032.
5. **Choi VW, Samulski RJ, McCarty DM.** 2005. Effects of adeno-associated virus DNA hairpin structure on recombination. J. Virol. **79**:6801–6807.
6. **Clemente R, de la Torre JC.** 2009. Cell entry of Borna disease virus follows a clathrin-mediated endocytosis pathway that requires Rab5 and microtubules. J. Virol. **83**:10406–10416.
7. **de Bruin K, et al.** 2007. Cellular dynamics of EGF receptor-targeted synthetic viruses. Mol. Ther. **15**:1297–1305.
8. **Desai A, Mitchison TJ.** 1997. Microtubule polymerization dynamics. Annu. Rev. Cell Dev. Biol. **13**:83–117.
9. **Ding W, Zhang LN, Yeaman C, Engelhardt JF.** 2006. rAAV2 traffics through both the late and the recycling endosomes in a dose-dependent fashion. Mol. Ther. **13**:671–682.
10. **Dodding MP, Way M.** 2011. Coupling viruses to dynein and kinesin-1. EMBO J. **30**:3527–3539.
11. **Douar AM, Poulard K, Stockholm D, Danos O.** 2001. Intracellular trafficking of adeno-associated virus vectors: routing to the late endosomal compartment and proteasome degradation. J. Virol. **75**:1824–1833.
12. **Duan D, et al.** 1999. Dynamin is required for recombinant adeno-associated virus type 2 infection. J. Virol. **73**:10371–10376.
13. **Dudleenamjil E, et al.** 2010. Bovine parvovirus uses clathrin-mediated endocytosis for cell entry. J. Gen. Virol. **91**:3032–3041.
14. **Engelke MF, Burckhardt CJ, Morf MK, Greber UF.** 2011. The dynactin complex enhances the speed of microtubule-dependent motions of adenovirus both towards and away from the nucleus. Viruses **3**:233–253.
15. **Gilbert J, Benjamin T.** 2004. Uptake pathway of polyomavirus via ganglioside GD1a. J. Virol. **78**:12259–12267.
16. **Greber UF, Way M.** 2006. A superhighway to virus infection. Cell **124**: 741–754.
17. **Greber UF, Willetts M, Webster P, Helenius A.** 1993. Stepwise dismantling of adenovirus 2 during entry into cells. Cell **75**:477–486.
18. **Grieger JC, Choi VW, Samulski RJ.** 2006. Production and characterization of adeno-associated viral vectors. Nat. Protoc. **1**:1412–1428.
19. **Grieger JC, Snowdy S, Samulski RJ.** 2006. Separate basic region motifs within the adeno-associated virus capsid proteins are essential for infectivity and assembly. J. Virol. **80**:5199–5210.
20. **Grieshaber SS, Grieshaber NA, Hackstadt T.** 2003. Chlamydia trachomatis uses host cell dynein to traffic to the microtubule-organizing center in a p50 dynamitin-independent process. J. Cell Sci. **116**:3793–3802.
21. **Hirosue S, et al.** 2007. Effect of inhibition of dynein function and microtubule-altering drugs on AAV2 transduction. Virology **367**:10–18.
22. **Huotari J, Helenius A.** 2011. Endosome maturation. EMBO J. **30**:3481–3500.
23. **Johnson JS, et al.** 2010. Mutagenesis of adeno-associated virus type 2 capsid protein VP1 uncovers new roles for basic amino acids in trafficking and cell-specific transduction. J. Virol. **84**:8888–8902.
24. **Johnson JS, Samulski RJ.** 2009. Enhancement of adeno-associated virus

infection by mobilizing capsids into and out of the nucleolus. J. Virol. **83**:2632–2644.
25. **Kelkar S, et al.** 2006. A common mechanism for cytoplasmic dynein-dependent microtubule binding shared among adeno-associated virus and adenovirus serotypes. J. Virol. **80**:7781–7785.
26. **Lakadamyali M, Rust MJ, Babcock HP, Zhuang X.** 2003. Visualizing infection of individual influenza viruses. Proc. Natl. Acad. Sci. U. S. A. **100**:9280–9285.
27. **Leopold PL, et al.** 1998. Fluorescent virions: dynamic tracking of the pathway of adenoviral gene transfer vectors in living cells. Hum. Gene Ther. **9**:367–378.
28. **Leopold PL, et al.** 2000. Dynein- and microtubule-mediated translocation of adenovirus serotype 5 occurs after endosomal lysis. Hum. Gene Ther. **11**:151–165.
29. **Leopold PL, Pfister KK.** 2006. Viral strategies for intracellular trafficking: motors and microtubules. Traffic **7**:516–523.
30. **Maguire AM, et al.** 2008. Safety and efficacy of gene transfer for Leber's congenital amaurosis. N. Engl. J. Med. **358**:2240–2248.
31. **McCarty DM, Monahan PE, Samulski RJ.** 2001. Self-complementary recombinant adeno-associated virus (scAAV) vectors promote efficient transduction independently of DNA synthesis. Gene Ther. **8**:1248–1254.
32. **Mellman I, Fuchs R, Helenius A.** 1986. Acidification of the endocytic and exocytic pathways. Annu. Rev. Biochem. **55**:663–700.
33. **Nathwani AC, et al.** 2011. Adenovirus-associated virus vector-mediated gene transfer in hemophilia B. N. Engl. J. Med. **365**:2357–2365.
34. **Neumann AK, Thompson NL, Jacobson K.** 2008. Distribution and lateral mobility of DC-SIGN on immature dendritic cells—implications for pathogen uptake. J. Cell Sci. **121**:634–643.
35. **Ohkawa T, Volkman LE, Welch MD.** 2010. Actin-based motility drives baculovirus transit to the nucleus and cell surface. J. Cell Biol. **190**:187–195.
36. **Qing K, et al.** 1999. Human fibroblast growth factor receptor 1 is a co-receptor for infection by adeno-associated virus 2. Nat. Med. **5**:71–77.
37. **Quintyne NJ, et al.** 1999. Dynactin is required for microtubule anchoring at centrosomes. J. Cell Biol. **147**:321–334.
38. **Radtke K, et al.** 2011. Plus- and minus-end directed microtubule motors bind simultaneously to herpes simplex virus capsids using different inner tegument structures. PLoS Pathog. **6**:e1000991. doi:10.1371/journal.ppat.1000991.
39. **Rogers GL, et al.** 2011. Innate immune responses to AAV vectors. Front. Microbiol. **2**:194.
40. **Roohvand F, et al.** 2009. Initiation of hepatitis C virus infection requires the dynamic microtubule network: role of the viral nucleocapsid protein. J. Biol. Chem. **284**:13778–13791.
41. **Sanlioglu S, et al.** 2000. Endocytosis and nuclear trafficking of adeno-associated virus type 2 are controlled by rac1 and phosphatidylinositol-3 kinase activation. J. Virol. **74**:9184–9196.
42. **Schroer TA.** 2004. Dynactin. Annu. Rev. Cell Dev. Biol. **20**:759–779.
43. **Schuh M.** 2011. An actin-dependent mechanism for long-range vesicle transport. Nat. Cell Biol. **13**:1431–1436.
44. **Snyder A, Wisner TW, Johnson DC.** 2006. Herpes simplex virus capsids are transported in neuronal axons without an envelope containing the viral glycoproteins. J. Virol. **80**:11165–11177.
45. **Sodeik B, Ebersold MW, Helenius A.** 1997. Microtubule-mediated transport of incoming herpes simplex virus 1 capsids to the nucleus. J. Cell Biol. **136**:1007–1021.
46. **Sonntag F, Bleker S, Leuchs B, Fischer R, Kleinschmidt JA.** 2006. Adeno-associated virus type 2 capsids with externalized VP1/VP2 trafficking domains are generated prior to passage through the cytoplasm and are maintained until uncoating occurs in the nucleus. J. Virol. **80**:11040–11054.
47. **Suikkanen S, et al.** 2003. Exploitation of microtubule cytoskeleton and dynein during parvoviral traffic toward the nucleus. J. Virol. **77**:10270–10279.
48. **Summerford C, Bartlett JS, Samulski RJ.** 1999. AlphaVbeta5 integrin: a co-receptor for adeno-associated virus type 2 infection. Nat. Med. **5**:78–82.
49. **Summerford C, Samulski RJ.** 1998. Membrane-associated heparan sulfate proteoglycan is a receptor for adeno-associated virus type 2 virions. J. Virol. **72**:1438–1445.
50. **Tsai MY, Morfini G, Szebenyi G, Brady ST.** 2000. Release of kinesin from vesicles by hsc70 and regulation of fast axonal transport. Mol. Biol. Cell **11**:2161–2173.
51. **Van de Walle GR, Favoreel HW, Nauwynck HJ, Van Oostveldt P, Pensaert MB.** 2001. Involvement of cellular cytoskeleton components in antibody-induced internalization of viral glycoproteins in pseudorabies virus-infected monocytes. Virology **288**:129–138.
52. **Vonderheit A, Helenius A.** 2005. Rab7 associates with early endosomes to mediate sorting and transport of Semliki forest virus to late endosomes. PLoS Biol. **3**:e233. doi:10.1371/journal.pbio.0030233.
53. **Wang J, Faust SM, Rabinowitz JE.** 2011. The next step in gene delivery: molecular engineering of adeno-associated virus serotypes. J. Mol. Cell. Cardiol. **50**:793–802.
54. **Wu Z, Asokan A, Samulski RJ.** 2006. Adeno-associated virus serotypes: vector toolkit for human gene therapy. Mol. Ther. **14**:316–327.
55. **Xiao PJ, Li C, Neumann A, Samulski RJ.** 2012. Quantitative 3D tracing of gene-delivery viral vectors in human cells and animal tissues. Mol. Ther. **20**:317–328.
56. **Zhao W, et al.** 2006. Role of cellular FKBP52 protein in intracellular trafficking of recombinant adeno-associated virus 2 vectors. Virology **353**:283–293.